Talanta 88 (2012) 160–167

Contents lists available at SciVerse ScienceDirect

Talanta

journal homepage: www.elsevier.com/locate/talanta

A micro GC detector array based on chemiresistors employing various surface functionalized monolayer-protected gold nanoparticles

Rih-Sheng Jian [a], Rui-Xuan Huang [b], Chia-Jung Lu [a,*]

[a] Department of Chemistry, National Taiwan Normal University, Taipei 11677, Taiwan, ROC
[b] Department of Chemistry, Fu-Jen Catholic University, Hsinchuang, Taiwan, ROC

ARTICLE INFO

Article history:
Received 17 August 2011
Received in revised form 15 October 2011
Accepted 20 October 2011
Available online 25 October 2011

Keywords:
micro-GC
Vapor sensor
MEMS
Chemiresistor
Volatile organic compounds

ABSTRACT

Aspects of the design, fabrication, and characterization of a chemiresistor type of microdetector for use in conjunction with gas chromatograph are described. The detector was manufactured on silicon chips using microelectromechanical systems (MEMS) technology. Detection was based on measuring changes in resistance across a film comprised of monolayer-protected gold nanoclusters (MPCs). When chromatographic separated molecules entered the detector cell, the MPC film absorbed vapor and undergoes swelling, then the resistance changes accordingly. Thiolates were used as ligand shells to encapsulate the nano-gold core and to manipulate the selectivity of the detector array. The dimensions of the μ-detector array were 14(L) × 3.9(W) × 1.2(H) mm. Mixtures of eight volatile organic compounds with different functional groups and volatility were tested to characterize the selectivity of the μ-detector array. The detector responses were rapid, reversible, and linear for all of the tested compounds. The detection limits ranged from 2 to 111 ng, and were related to both the compound volatility and the selectivity of the surface ligands on the gold nanoparticles. Design and operation parameters such as flow rate, detector temperature, and width of the micro-fluidic channel were investigated. Reduction of the detector temperature resulted in improved sensitivity due to increased absorption. When a wider flow channel was used, the signal-to-noise ratio was improved due to the larger sensing area. The extremely low power consumption and small size makes this μ-detector array potentially useful for the development of integrated μ-GC.

© 2011 Elsevier B.V. All rights reserved.

1. Introduction

Portable gas chromatographs or micro-gas chromatographs (μ-GCs) provide an analytical tool that permits the rapid analysis of volatile organic compounds (VOC) in the environment. In contrast with benchtop gas chromatographs, the goal of which is more complete separation using longer columns or lower detection limits using a mass spectrometer as the detector, the goal when using a μ-GC is to achieve portability and rapid analyses for field applications such as contamination surveys, industrial hygiene, and homeland security [1–5].

Commercially, so-called "micro" GCs are in fact compact and portable versions of regular benchtop GCs. However, academic researchers often refer to μ-GC as employing microfabrication technologies that are intended to achieve miniaturization, with the ultimate objective of developing a GC-on-a-chip. The realization of a GC-on-a-chip has become an ongoing quest for analytical scientists since the first report of such a device by Terry et al. [6]. The device was a wet-etched (i.e., using KOH solution to etch a silicon wafer) separation channel with a single metal-deposited thermal conductivity detector (TCD) on a 4 in. silicon wafer, which had the capacity to separate and detect a limited number of gases with the aid of off-chip facilities (e.g., gas cylinder, power supply, and electronics). However, with the advancing development of MEMS technology, many new fabrication processes and devices are now available for Lab-on-chip development and chemical detection [7–9].

For the past three decades, many researchers have been interested in developing MEMS components for μ-GCs such as micro-valves [10–12], micro-columns [13–15] and micro-preconcentrators [16–20]. In addition, several reports have appeared regarding the integration of a fully functional hybrid μ-GC using a combination of MEMS and non-MEMS devices [21–25].

Microdetectors play a crucial role in achieving high performance μ-GC, in that they are major determinants of the detection limits of a μ-GC system. Several micro detectors for GC have been previously reported, such as μ-TCD [26,27], μ-plasma detectors [28] and

* Corresponding author. Tel.: +886 2 77346132; fax: +886 2 29324249.
E-mail address: cjlu@ntnu.edu.tw (C.-J. Lu).

0039-9140/$ – see front matter © 2011 Elsevier B.V. All rights reserved.
doi:10.1016/j.talanta.2011.10.025

μ-FID [29–32], the very recent works of miniaturized FID (i.e., flame ionization detector) reported by Kuipers [31] and Guan [32] that shows promising sensitivity for further applications. If the μ-GC is designed to perform long-term field analysis where a continuous auxiliary gas supply might be limited, VOC sensors become a rational choice. MEMS fabricated metal oxide sensors (e.g., catalyst doped SnO_2 or TiO_2) have shown the potential to be highly sensitive detectors that do not require auxiliary gases [25,33,34]. Unfortunately, this type of sensor requires high temperature (e.g., 300 °C or above) for operation, which inevitably drains the energy from μ-GC system batteries and limits the time for continuous field analyses. Other gas sensors such as piezoelectric- or conductive-type sensors coated with modified carbon nano-tubes for VOC detection without the requirement of heating have also been explored recently [35,36].

A chemiresistor using monolayer-protected gold nanoclusters (MPCs) as a sensing film is another type of VOC sensor that can operate directly at room temperature. A procedure for the synthesis of this material was first reported by Brust [37,38], and interest developed almost instantly because of its versatile properties in optics, electrochemistry and surface reactions [39,40]. The use of MPC chemiresistors for VOC detection was pioneered by Wohltjen and Snow [41,42]. In addition to the measurement of changes in resistance, vapor detection using MPCs as a chemically sensitive film have also been demonstrated with localized surface plasmon resonance (LSPR) sensors and quartz crystal microbalance (QCM) [43–46].

The response signal of a MPC chemiresistor is obtained by measuring the current of electron tunneling or hopping between neighboring gold cores within a MPC film [47,48]. Vapor absorption swells the film, which increases the distance between the gold cores. The mechanism [49] can be described by the following expression for the conductivity of the film, σ:

$$\sigma \propto e^{(-\beta\delta)} e^{(-E_a/k_B T)} \quad (1)$$

where β is the electron tunneling constant, which is related to the dielectric properties of the organic layer between the gold cores, δ is the edge-to-edge separation of the metal core, E_a is the activation energy, k_B is the Boltzmann constant, and T is the absolute temperature. Steinecker and Zellers further developed a response model for VOC sensing that incorporates parameters such as the volatility, dielectric constant, and free volume of absorbed vapor molecules [50].

We previously reported that the VOC-sensing selectivity of a MPC chemiresistor can be tuned through the functional group of the organic thiolate on the gold nanoparticles [51], and found that Polarity or π electron rings on a surface ligand have a pronounced effect on sensor selectivity. Zhong et al. also investigated the VOC responses of several cross-linked MPCs with different surface ligands, and tested the pattern recognition based on array responses [52–54]. Cai and Zellers reported on the first GC detector using a dual chemiresistor with two different thiolates (*n*-octanethiol and 2-phenylethanethiol), which were used to cap MPCs. The detector was sealed within a hand-made glass cell with an internal volume of ~60 μL [55].

As part of an effort to design a fully integrated μ-GC, this paper describes the design, fabrication, and evaluation of a μ-detector based on a chemiresistor array of 4 different monolayer-protected gold nanoparticles. Both the flow-through channel and the sensing electrodes were fabricated on silicon chips using MEMS technology. The reasons and concepts for the design of the chemical structure of four sensing materials are discussed. The influences of internal dimension, flow velocity and temperature on the μ-detector performances were evaluated.

2. Experimental

2.1. Chemicals

Deionized water was produced using a Millipore Bedford system. Hydrogen tetrachloroaurate ($HAuCl_4$) was obtained from Alfa Aesar, UK. Tetraoctylammonium bromide (TOAB) and other organic thiolates such as *n*-octanethiol, Isooctyl 3-mercapropionate, 3-mercaptopropionic acid and 4-pyridinethiol were obtained from Acros. All organic solvents used to generate test vapor were HPLC reagent grade or higher.

2.2. Sensing material synthesis

MPCs were synthesized using the two-phase approach reported by Brust et al. [37,38]. The four different surface monolayers of thiolates selected for capping gold nanoparticles were as follows: *n*-octanethiol (Au-C8), isooctyl 3-mercapropionate (Au-EST), a mixture of *n*-octanethiol and 3-mercaptopropionic acid (Au-C8PA), and a mixture of *n*-octanethiol and 4-pyridinethiol (Au-C8Py). The chemical structures of the 4 MPCs are shown in Fig. 1. The synthetic approach for preparing the two pure ligand MPCs, Au-C8 and Au-EST, was as follows: 0.10 g of $HAuCl_4$ was dissolved in 8 mL of deionized water, and 0.16 g of TOAB and 17 μL of *n*-octanethiol or isooctyl 3-mercapropionate were dissolved in 40 mL of toluene. The aqueous $HAuCl_4$ solution was added to the TOAB/toluene solution, and the resulting mixture was stirred for 15 min. The yellow-colored $HAuCl_4$ was transferred from the aqueous solution to the toluene. A reducing agent prepared by dissolving 0.112 g of $NaBH_4$ in 8 mL of water was added to the stirred mixture of toluene/water solutions. A rapid color change from yellow to deep purple developed immediately. Vigorous stirring was continued for 1 h at room temperature. Discussions regarding the synthetic parameters can be found in several previous reports [41,42]. MPCs with mixed thiolate shells (i.e., Au-C8PA and Au-C8Py) were synthesized via a ligand place-exchange reaction [56,57] of *n*-octanethiol with 3-mercaptopropionic acid or 4-pyridinethiol. A 0.2 μL aliquot of 3-mercaptopropionic acid or 4-pyridinethiol was added to the Au-C8/toluene solution and the resultant solution was stirred for 3 h. Further purification was achieved by re-precipitating the MPCs in a large quantity of cold ethanol to remove excess TOAB or thiolates. The evidence of nanostructures, such as TEM images and UV–vis spectra, have been reported elsewhere [51]. The final products were re-dissolved in toluene and dried using a rotary evaporator for further use.

2.3. Fabrication of chips

The μ-detector consisted of two chips: sensing electrodes and micro-fluidic chambers. Fig. 2 shows the schematic design and a photo of the actual devices. The micro-fluidic chambers were fabricated by deep-reactive-ion-etch (DRIE) in designed patterns. The patterns were defined on silicon wafers through a regular photolithography approach and RU-8 photoresistor. The width and depth of the inlet and outlet of the fluidic channel were 380 μm × 380 μm, which allowed deactivated capillary tubes (250 μm i.d. Supelco Inc., USA) to be inserted. Three different widths of detector chambers, (A) 1.5, (B) 0.75 and (C) 0.35 mm, were fabricated to observe the effect of flow channel width versus detector performance. To leave room for electrical connection pins, 8 grooves were etched on both sides. The calculated internal volumes of the detection chambers were 5.3, 2.5, 1.2 μL, respectively. The sensing electrodes consisted of 4 interdigital microelectrode pairs fabricated by a lift-off process. Each microelectrode consisted of 40 pairs of interdigital gold fingers that were 1.5 mm in length, 15 μm in width and were separated by 10 μm. The thickness of the

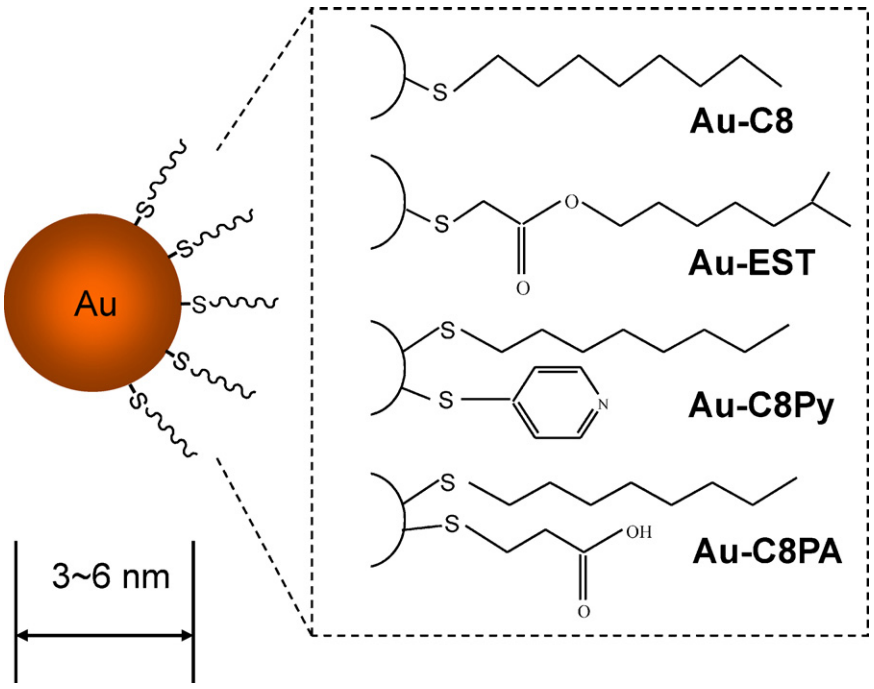

Fig. 1. Chemical structures of monolayer protected gold nanoclusters for the chemiresistor array.

gold electrode film was 300 nm, which was sputtered on Si substrates using a thin Cr (5 nm) layer for adhesion. The active area of each pair of microelectrodes was 3 mm^2. The overall size of this μ-detector was smaller than a one-cent coin (Fig. 2).

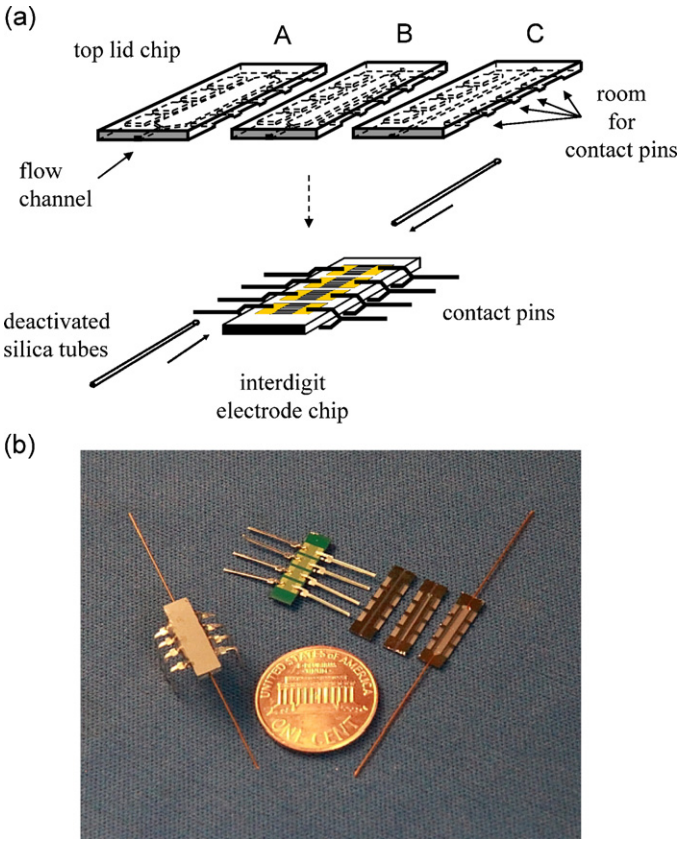

Fig. 2. Design diagram and photograph of the μ-detector.

2.4. Coating and packaging of the μ-detector

The surface of the interdigital electrode was treated with 1/3: H_2O_2 (30%)/H_2SO_4 to remove possible residual contaminants, rinsed with deionized water and high purity ethanol, and then dried in an oven at a temperature of 100 °C. The substrates were then exposed to the saturated vapor of hexamethylsiloxane by placing it in a small vial (20 mL) sealed with a few drops of hexamethylsiloxane for 8 h. After the reaction with hexamethylsiloxane, the devices were removed from the vial, cleaned with ethanol and blow-dried with N_2. The surface of the Si substrate was converted to a hydrophobic state for better adhesion of the MPC films. The MPCs were re-dissolved in dichloroethane and spray-coated with a precise airbrush using high-purity nitrogen as the carrier gas. The previously reported thickness uniformity of spray-coated film was examined by SEM image [51]. The resistance of the MPC film was monitored throughout the coating process using a high-resistance meter (picoampermeter 6478, Keithley Instruments Inc., Cleveland, OH).

The top lid (micro-fluidic chamber) was pressed tightly on the electrode array chip by a string clip. Deactivated capillary tubes of 250 μm i.d. were inserted into the inlet and outlet ports. Half-dried epoxy resin was applied around the outer rim of the device and allowed to dry at room temperature. The string clip was removed after the device had been completely sealed by the epoxy resin. A minimum flow (~1 mL/min) of N_2 was continuously purged through the detection chamber during the sealing process to prevent the MPC film from being contaminated by the solvent evaporating from the drying epoxy.

2.5. Instrumentation of the test system

The test system was constructed on a HP 5890 GC-FID. The μ-detector was connected to the capillary column by means of a Y-glass connector (GlasSeal™, Supelco Co., USA) in parallel with the FID, as shown in Fig. 3. Test mixtures of 8 vapors at a concentration range of 2000–5000 ppm were generated in Tedlar bags. Aliquots of 0.1–0.5 mL vapor samples, equivalent to a mass that

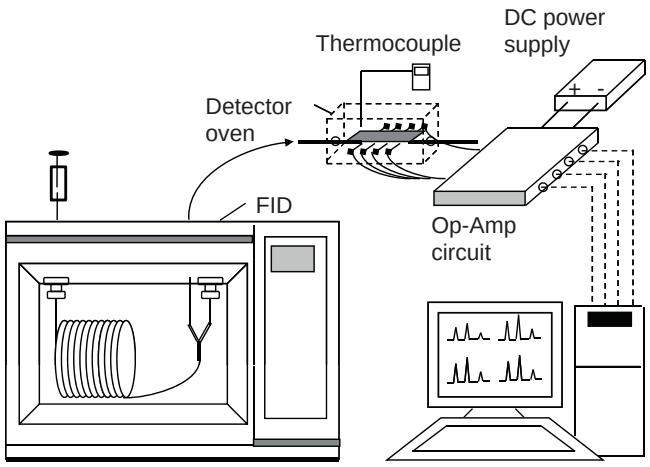

Fig. 3. Experimental system for testing the μ-detector.

ranged from 0.5 to 10 μg, were injected into the GC using a gas-tight syringe. Zero air was used as the carrier gas and flow rates ranging from 2.0 to 10.0 mL/min were tested. The vapor mixtures were separated by a DB-1 capillary column (30 m × 0.53 mm i.d., 1.5 μm film thickness, Supelco, USA). The temperature program was set initially at 50 °C for 1 min and then ramped up to 120 °C at a rate of 20 °C/min. Separated compounds eluted from the column were simultaneously detected by FID and the μ-detector. The μ-detector was placed in a small oven at 25, 35 or 45 °C to test the effect of temperature on the detector.

A ±5 V DC power supplier and a low-pass filter with a differential amplifier circuit of four channels were used to drive the μ-detector. Voltage output signals were recorded through a data acquisition card (NI-4472, National Instruments, TX) and stored on a personal computer. Data acquisition software was written in-house, using LabVIEW (National Instrument) software.

3. Results and discussion

3.1. Chromatographic responses of the μ-detector

Fig. 4 shows five chromatograms (one FID and four μ-chemiresistor channels) that were observed for a single injection of 8 VOC mixtures. Since the mixture sample was prepared and

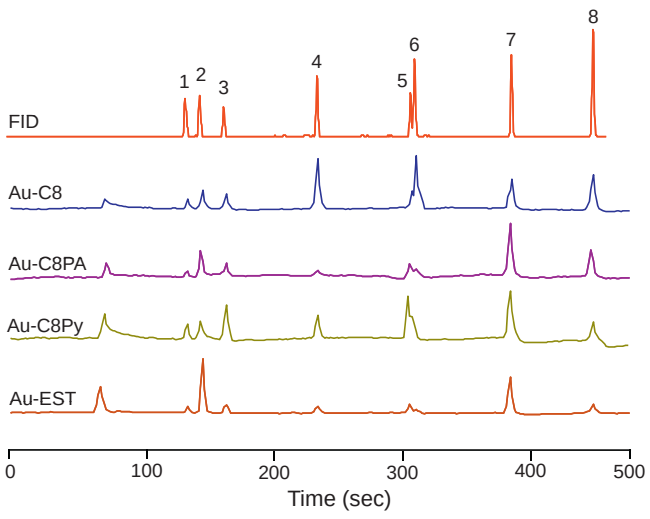

Fig. 4. Chromatograms of the same injection detected by both a FID and the μ-detector.

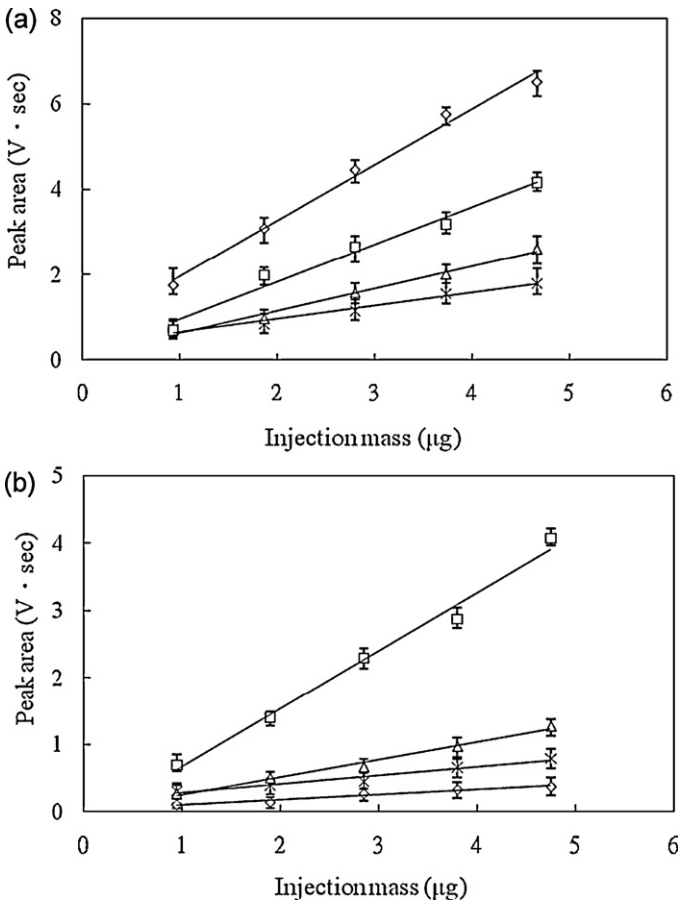

Fig. 5. Calibration curves for (a) *n*-octane and (b) butyl acetate. (◊: Au-C8, □: Au-C8Py, △: Au-C8PA, × Au-EST.) Error bars indicate the highest and lowest responses that were obtained for three replicated measurements at the same concentration level.

injected directly from the gas phase, no solvent peak was detected by the FID. The injection mass for each compound in this chromatogram was as follows: 1,2-dichloroethane 6.1 μg, *n*-butanol 4.5 μg, 1,4-dioxane 2.2 μg, toluene 2.3 μg, butyl acetate 2.9 μg, *n*-octane 2.8 μg, 2-heptanone 2.8 μg, and anisole 2.7 μg. It is interesting that all four channels of the μ-detector showed an extra and non-retained peak in their chromatograms. We believe that this is from humidity that permeated into the Tedlar bag during the time the sample was sitting in the lab prior to injection.

Another major difference is that the peak widths of the μ-detector were all broader than that of the FID. This can be attributed to two factors: the internal volume of the μ-detector and the finite time required for vapor to diffuse into the MPC films. When the MPCs were spray-coated to form a thin film on interdigit electrodes, these nanoparticles were closely packed and the outer shell thiolates were overlapped to form an organic phase. The vapor molecules eluted from the column were absorbed and diffused into the film. The preference of the partition was then determined by the solvation interaction between thiolate shells and incoming vapor molecules. The initial selectivity of the μ-chemiresistor array can be seen by comparing peak 5 (butyl acetate) and peak 6 (*n*-octane) in Fig. 4. The detector channel coated with Au-C8 showed a relative higher response to *n*-octane, while all three of the others showed much smaller responses. Fig. 5 shows calibration curves for *n*-octane and butyl acetate when they were injected separately. Each calibration was performed at five different injection masses and three replicates of the same injection mass. Generally good linearity was observed, and R^2 values were in the range of 0.990–0.999

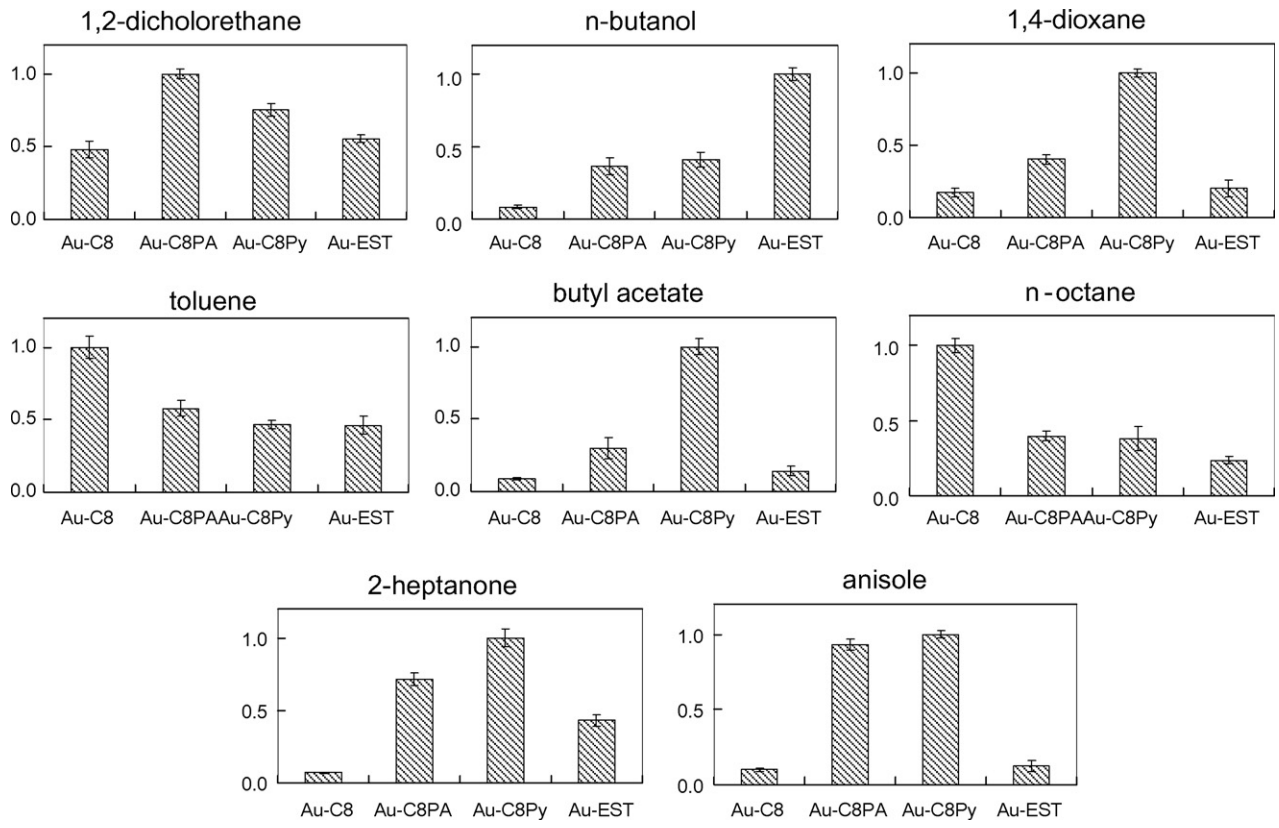

Fig. 6. Response patterns of the 8 VOCs tested using the μ-detector array.

for calibration curves. The equivalent average concentrations calculated by dividing injection mass by peak volume were converted into ppm (v/v) and ranged from 187 to 936 ppm for *n*-octane and 244 to 1220 ppm for butyl acetate.

3.2. Material structure design and chemical selectivity

Fig. 6 shows the response patterns for the eight tested compounds for the μ-chemiresistor array. The response patterns were plotted in such a way that the highest sensitivity (i.e., calibration slope) of each compound in the array was normalized to unity. As this figure shows, these patterns allow the 8 tested vapors to be divided into several sub-groups. In this detector array, Au-C8 was chosen because of its tendency to be more sensitive to non-polar organics. This is because the ligand overlap regions between adjacent Au-C8 nanoparticles are saturated hydrocarbon chains that allow non-polar molecules (i.e., *n*-octane or toluene) to be partitioned within them and effectively cause MPC film swelling. If a polar compound such as *n*-butanol were to be absorbed in this film, it would less favorable to partitioning within a non-polar region.

Au-EST has an ester functional group (Au-S-CH2-COO-R′, Fig. 1) within the shell overlap region, which can greatly assist in the absorption of polar compounds. As a result, the detection of *n*-butanol on the Au-EST-coated chemiresistor showed a much higher sensitivity than that of the Au-C8 chemiresistor. A nonpolar chain on the outer shell (R′) of Au-EST is also necessary for high sensitivity in resistance changes, because it reduces interparticle attractions between polar functional groups of adjacent nanoparticles that could inhibit swelling.

Initially, we attempted to expand the design concept of the Au-EST to other polar groups, such as hydrogen bond donor functionalities. However, thiolates with such structures are not readily available. Instead, we adapted the mixed-ligand concept previously demonstrated by Kim et al. [57], who observed selectivity changes after partially replacing octanethiol with chlorobenzenethiol on the MPC surface. In the present study, 3-mercaptopropionic acid (PA) and 4-pyridinethiol (Py) were used in the exchange reaction to alter the surface chemical affinity of MPCs. As can be seen in Fig. 6, the sensitivities of these two mixed-ligand sensors were much higher for the hydrogen-bond acceptors such as butyl acetate, 2-heptanone, etc. It is interesting to note that Au-C8Py functioned as a better hydrogen bond donor than Au-C8PA, as shown by a comparison of their sensitivities versus H-bond accepting compounds. This suggests that the nitrogen site on the pyridine ring must be protonated during the surface replacement reaction, resulting in a (R-N:H^+) strong H-bond donor at the end.

3.3. Flow velocity effects of μ-detectors

Fig. 7 shows the results for flow rate changes versus the sensitivity of the chemiresistor array for each compound. As can be seen in this figure, the selectivity remains roughly the same, but there is a common trend indicating the sensitivity is reduced with increasing flow rate. There are two factors that could cause this result. The first is the dilution in the concentration of the eluted peak at higher flow rates. Unlike the FID, which is a mass-flow detector, the MPC chemiresistor is a concentration-dependent detector based on the partition equilibrium between the mobile phase and the sensing film. A higher carrier flow rate would naturally result in a decrease in peak concentration when the sample was eluted through the column. This is different from testing with a dynamic vapor generation system. A previous study showed a raise in sensor response with increasing vapor flow rate while testing carbon-nanotube based chemiresistors.[58] The second factor is the insufficient diffusion time into the MPC film at high flow rates. This is similar to the non-equilibrium term (*Cs*) in the van Deemter equation. Zhong and

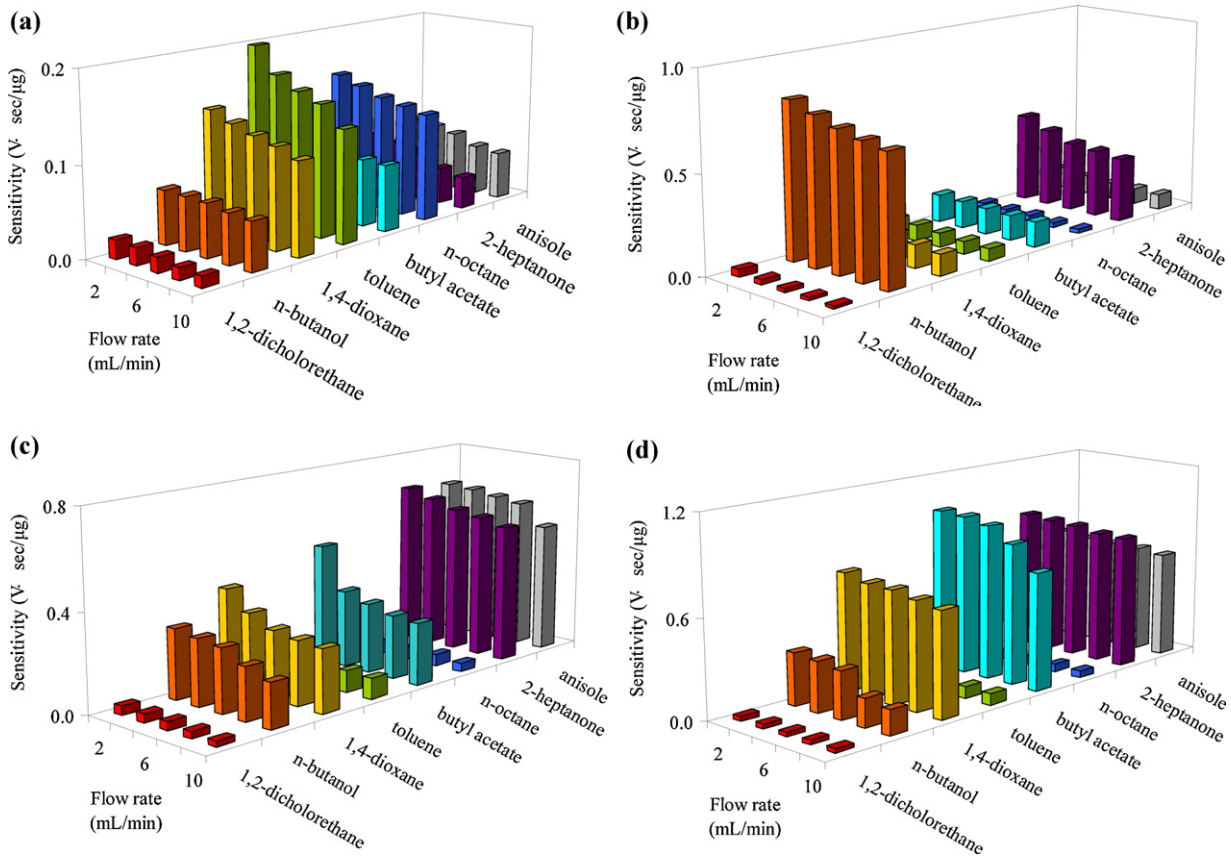

Fig. 7. Sensitivities of the μ-detector with different flow rates. Sensor coatings: (a)Au-C8, (b)Au-EST, (c)Au-C8PA, (d)Au-C8-Py.

Zellers [23] estimated that the diffusion time required for MPC film is roughly 0.02 s and concluded that this should result in an insignificant contribution in their devices, in which the detector residence time was 0.05–1 s. In the current study, as the detector chambers were miniaturized, the detector residence times were reduced to 0.006–0.03 s, which was significantly shorter than those used in previous reports. Therefore, we cannot rule out the possible influence at this time. However, a precise evaluation of non-equilibrium diffusion remains difficult, since the diffusion coefficient of a VOC through the MPC film is unknown.

3.4. Channel width effect of μ-detectors

Fig. 8a shows chromatograms for 3 different μ-detectors with different channel widths. The volumetric flow rates were the same (6 mL/min) to avoid discrepancies in concentration dilution among the different devices. The film thicknesses of three devices were controlled to be approximately the same by monitoring the film resistance during the coating process. However, due to differences in the detector channel width, the linear velocities and active sensing areas under the flow channel differed. The calculated linear velocities were 0.19, 0.38 and 0.84 m/s, and the active sensor areas were 14.25, 7.12 and 3.34 mm^2, respectively, for the devices labeled A, B and C (Fig. 2). As shown in Fig. 8, the devices with a wider flow channel or larger sensing area showed a higher response with the same injection mass. Fig. 8b shows a closeup of the toluene peaks in Fig. 8a chromatograms. Fig. 8c shows another set of partially overlapping peaks (butyl acetate and *n*-octane). It is clear that both peak height and width increased as the channel width was increased. There was also a slight delay in peak retention time as the channel width increased. Since the peak concentration was the same for these 3 tests, the improvement in peak height must be caused by two factors: the larger sensing area and slower linear velocity. The overall changes in film resistance would be greater if a larger film area was simultaneously exposed to vapor molecules. Slower gas velocity provides a longer residence time for mass diffusion into the MPC film. The retention delay and peak broadening for a wider channel device can be attributed to the larger internal volume, which would require a slightly longer mixing time to reach equilibrium concentration inside the detection chamber. The same trends for sensitivity change and peak broadening were consistent for all sensors and tested vapors. In summary, signal-to-noise ratio can be enhanced by using a larger sensing area and slower linear velocity of carrier gas for this μ-detector.

3.5. Temperature effect on a μ-detector

To observe the temperature effect on the μ-detector, it was placed in a thermostat-controlled box separate from the GC oven. We tested the same separation conditions with detector temperatures of 25, 35 and 45 °C. The chromatograms for the Au-C8 channel are shown in Fig. 9. It is obvious that the detector responses decreased as the temperature of the detector increased. Since the responses of this detector are based on the absorption of vapor molecules on the MPC film, an increase in detector temperature would result in reduced absorption. The inset shows a close-up of the toluene peaks at different temperatures. Response reductions were observed for all of the tested compounds.

Generally, an increase in temperature will increase the kinetic energy of molecules. Therefore, the diffusion "rate" will increase. In other words, gases permeate more easily into the film. However, the increase in kinetic energy also implies that VOC molecules tend to stay in the gas phase rather than being "condensed" (i.e., absorbed). The raise in temperature is favorable for a solid to be

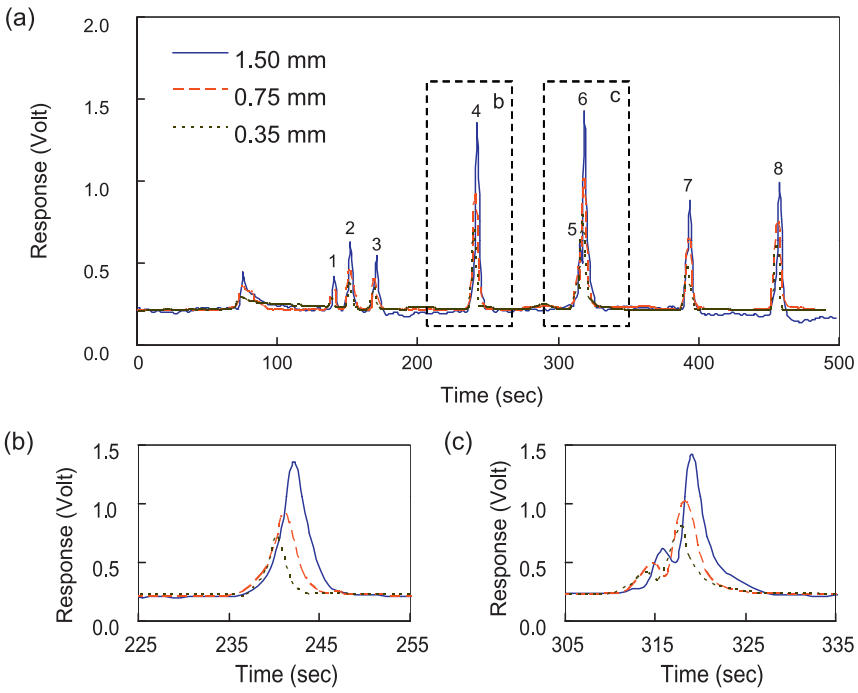

Fig. 8. Chromatograms of μ-detectors with different flow channel widths. (Channel width: device A: 1.5 mm, device B: 0.75 mm, device C: 0.35 mm.)

dissolved into liquid, but is less favorable for gases to be trapped in a condensed phase. Regarding the temperature effects on electron tunneling in MPC films, it has been thoroughly discussed [49,50]. The raise in temperature increased the conductivity of the film, as revealed in Eq. (1), but affected only the baseline resistance during our measurements since the detector was held at constant temperature during each chromatographic run. There was no temperature change between the background carrier gas and the sample zone reaching the detector. We measured the signal difference between carrier and sample zone under the same given temperatures (i.e., 25, 35, and 45 °C), and, hence, the same baseline resistance.

3.6. Detection limits

The detection limits of the μ-detector, tested at 25 °C, are listed in Table 1. The values were calculated by dividing a 3-fold baseline standard deviation (3σ) by the calibration slopes. The range of the detection limit was 2–111 ng. The trend for the detection limit was mainly determined by the volatilities of the compounds, with variations caused by chemical selectivity provided by the surface ligands of MPCs. Although we tested this array side-by-side with a FID, our objective was not to compete with the FID in terms of detection limits, which is typically in the range of a few pg/s. The key advantages of this detector are its small size and power conservation, which will permit its use in portable and battery powered μ-GC systems in the future.

The resistances of the MPC films used in the present study ranged from a few hundred kΩ to a few MΩ. The voltage required to drive this detector was only 1–5 V. Thus, the current consumed by this device was on the order of μA. Even the peripheral signal process electronics consumed more power than this μ-detector. The issue of power consumption is essential for future applications, if

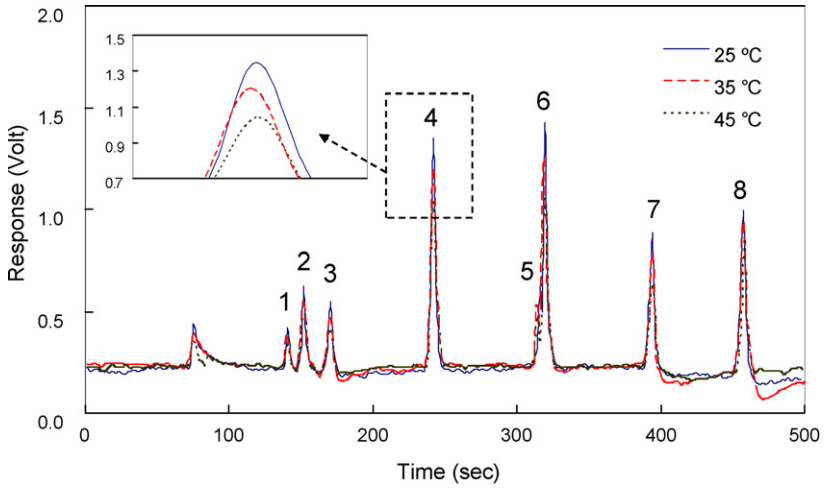

Fig. 9. Chromatograms of the Au-C8 μ-detector at 25, 35 and 45 °C.

Table 1
The detection limits of μ-detector array for 8 tested VOCs.

#	Compound	Vapor pressure (Pa) at 20 °C	Detection limits (ng, 3σ/slope)			
			Ag-C8	Au-C8PA	Au-C8Py	Au-EST
1	1,2-dicholorethane	8252.5	102	111	69	93
2	*n*-butanol	546.6	30	3	9	8
3	1,4-dioxane	3892.9	15	15	8	4
4	toluene	3799.6	10	30	26	33
5	butyl acetate	1039.8	22	16	8	3
6	*n*-octane	1386.5	13	70	46	48
7	2-heptanone	279.9	31	6	4	2
8	anisole	466.6	26	25	3	4

the size of the μ-GC system can be further reduced and batteries become a constraint to the duration of continuous operation.

4. Conclusion

This paper describes the design, fabrication and initial evaluation of a μ-detector array constructed on a silicon chip using MEMS technology, and using nanomaterials as the chemically responsive interface. The ultra small dimension, free from the need of auxiliary gases and low-power consumption, make this detector suitable for future integration with GC-on-chip. The sensing material design in the present study also showed sufficient selectivity to create response patterns for vapors with different functional groups. This feature provides additional qualitative information of analytes that cannot be obtained from a single, universal detector. Some design rules can be summarized based on the results from the present study. First, the flow channel should be designed as wide and shallow as possible to increase electrode area without overly increasing the internal volume. Second, the detector should be thermally stated due to its susceptibility to temperature change. The implantation of a cooling device would greatly enhance the sensitivity of this detector. Third, flow velocity through this detector should be reduced whenever possible, but must be a compromise with the GC carrier flow rate. The detection limit of this initially developed detector is not yet comparable to those of commercial detectors. Possible improvements through the use of new synthetic materials, geometric design of the device, and noise filtering circuits are currently underway.

Acknowledgement

The authors thank the National Science Council (NSC) of Taiwan, ROC for its funding support of this project under contract number NSC98-2113-M-003-005-MY2.

References

[1] A. Arora, G. Simone, G.B. Salieb-Beugelaar, J.T. Kim, A. Manz, Anal. Chem. 82 (2010) 4830.
[2] D.K.W. Wang, C.C. Austin, Anal. Bioanal. Chem. 386 (2006) 1089.
[3] S.I. Ohira, K. Toda, Anal. Chim. Acta 619 (2008) 143.
[4] X. Liu, J. Pawliszyn, Int. J. Environ. Anal. Chem. 85 (2005) 1189.
[5] F.J. Santos, M.T. Galceran, Trends Anal. Chem. 21 (2002) 672.
[6] S.C. Terry, J.H. Jerman, J.B. Angell, IEEE Trans. Electron Device 26 (1979) 1880.
[7] C. Karuwan, K. Sukthang, A. Wisitsoraat, D. Phokharatkul, V. Patthanasettakul, W. Wechsatol, A. Tuantranont, Talanta 84 (2011) 1384.
[8] M.M.R. Howlader, M.G. Kibria, F. Zhang, M.J. Kim, Talanta 82 (2010) 508.
[9] A. Jang, Z. Zou, K.K. Leeb, C.H. Ahnb, P.L. Bishopa, Talanta 83 (2010) 1.
[10] M. Nowak, A. Gorsuch, H. Smith, R. Sacks, Anal. Chem. 70 (1998) 2481.
[11] H. Erxleben, J. Ruzicka, Analyst 130 (2005) 469.
[12] M.D.L. de Castro, J. Ruiz-Jimenez, J.A. Perez-Serradilla, Trends Anal. Chem. 27 (2008) 118.
[13] G.R. Lambertus, A. Elstro, K. Sensenig, J. Potkay, M. Agah, S. Scheuering, K. Wise, F. Dorman, R. Sacks, Anal. Chem. 76 (2004) 2629–2637.
[14] G.R. Lambertus, C.S. Fix, S.M. Reidy, R.A. Miller, D. Wheeler, E. Nazarov, R. Sacks, Anal. Chem. 77 (2005) 7563–7571.
[15] M.A. Zareian-Jahromi, M. Ashraf-Khorassani, L.T. Taylor, M. Agah, J. Microelectromech. Syst. 18 (2009) 28.
[16] C.J. Lu, E.T. Zellers, Analyst 127 (2002) 1061.
[17] C.J. Lu, E.T. Zellers, Anal. Chem. 73 (2001) 3449.
[18] W.C. Tian, S.W. Pang, C.J. Lu, E.T. Zellers, J. Microelectromech. Syst. 12 (2003) 264.
[19] I. Voiculescu, M. Zaghloul, N. Narasimhan, Trends Anal. Chem. 27 (2008) 327.
[20] B. Alfeeli, M. Agah, IEEE Sens. J. 9 (2009) 1068.
[21] C.J. Lu, W.H. Steinecker, W.C. Tian, M.C. Oborny, J.M. Nichols, M. Agah, J.A. Potkay, H.K.L. Chan, J. Driscoll, R.D. Sacks, K.D. Wise, S.W. Pang, E.T. Zellers, Lab Chip 5 (2005) 1123.
[22] M. Agah, G.R. Lambertus, R. Sacks, K. Wise, J. Microelectromech. Syst. 15 (2006) 1371.
[23] Q. Zhong, W.H. Steinecker, E.T. Zellers, Analyst 134 (2009) 283.
[24] P.R. Lewis, P. Manginell, D.R. Adkins, R.J. Kottenstette, D.R. Wheeler, S.S. Sokolowski, D.E. Trudell, J.E. Byrnes, M. Okandan, J.M. Bauer, R.G. Manley, C. Frye-Mason, IEEE Sens. J. 6 (2006) 784.
[25] S. Zampolli, I. Elmi, F. Mancarella, P. Betti, E. Dalcanale, G.C. Cardinali, M. Severi, Sens. Actuators B 141 (2009) 322.
[26] D. Cruz, J.P. Chang, S.K. Showalter, F. Gelbard, R.P. Manginell, M.G. Blain, Sens. Actuators B 121 (2007) 414.
[27] J.A. Dziuban, J. Mrozb, M. Szczygielska, M. Malachowski, A. Gorecka-Drzazga, R. Walczak, W. Bula, D. Zalewski, L. Nieradko, J. Lysko, J. Koszur, P. Kowalski, Sens. Actuators A 115 (2004) 318.
[28] Y.M. Fu, S.C. Chu, C.J. Lu, Microchem. J. 89 (2008) 7–12.
[29] S. Zimmermann, P. Krippner, A. Vogel, J. Muller, Sens. Actuators B 83 (2002) 285.
[30] S. Zimmermann, S. Wischhusen, J. Muller, Sens. Actuators B 63 (2000) 159.
[31] W. Kuipers, J. Muller, Talanta 82 (2010) 1674.
[32] J. Wang, H. Wang, C. Duan, Y. Guan, Talanta 82 (2010) 1022.
[33] I. Simon, N. BaArsan, M. Bauer, U. Weimar, Sens. Actuators B 73 (2001) 1.
[34] S. Zampolli, I. Elmi, J. Sturmann, S. Nicoletti, L. Dori, G.C. Cardinali, Sens. Actuators B 105 (2005) 400.
[35] B. Pejcic, M. Myersa, N. Ranwala, L. Boyd, M. Baker, A. Ross, Talanta 85 (2011) 1648.
[36] B. Kumar, J.-F. Feller, M. Castro, J. Lu, Talanta 81 (2010) 908.
[37] M. Brust, M. Walker, D. Bethell, D. Schiffrin, R. Whyman, J. Chem. Soc. Chem. Commun. (1994) 801.
[38] M. Brust, J. Fink, D. Bethella, D.J. Schiffrina, C. Kiely, J. Chem. Soc. Chem. Commun. (1995) 1655.
[39] R. Sardar, A.M. Funston, P. Mulvaney, R.W. Murray, Langmuir 25 (2009) 13840.
[40] R.W. Murray, Chem. Rev. 108 (2008) 2688.
[41] H. Wohltjen, A.W. Snow, Anal. Chem. 70 (1998) 2856.
[42] A.W. Snow, H. Wohltjen, Chem. Mater. 10 (1998) 947.
[43] C.S. Cheng, Y.Q. Chen, C.J. Lu, Talanta 73 (2007) 358.
[44] Y.Q. Chen, C.J. Lu, Sens. Actuators B 135 (2009) 492.
[45] K.J. Chen, C.J. Lu, Talanta 81 (2010) 1670.
[46] C.L. Li, C.J. Lu, Talanta 79 (2009) 851.
[47] T. Sato, H. Ahmed, D. Brown, B.F.G. Johnson, J. Appl. Phys. 82 (1997) 696.
[48] W.P. Wuelfing, S.J. Green, J.J. Pietron, D.E. Cliffel, R.W. Murray, J. Am. Chem. Soc. 122 (2000) 11465.
[49] F.P. Zamborini, L.E. Smart, M.C. Leopold, R.W. Murray, Anal. Chim. Acta 496 (2003) 3.
[50] W.H. Steinecker, M.P. Rowe, E.T. Zellers, Anal. Chem. 79 (2007) 4977.
[51] C.Y. Yang, C.L. Li, C.J. Lu, Anal. Chim. Acta 565 (2006) 17.
[52] L. Wang, X. Shi, N.N. Kariuki, M. Schadt, G.R. Wang, Q. Rendeng, J. Choi, J. Luo, S. Lu, C.J. Zhong, J. Am. Chem. Soc. 129 (2007) 2161.
[53] L. Han, D.R. Daniel, M.M. Maye, C.J. Zhong, Anal. Chem. 73 (2001) 4441.
[54] L. Han, X. Shi, W. Wu, F. Louis Kirk, J. Luo, L. Wang, D. Mott, L. Cousineau, S. I-Im Lim, S. Lu, C.J. Zhong, Sens. Actuators B 106 (2005) 431.
[55] Q.Y. Cai, E.T. Zellers, Anal. Chem. 74 (2002) 3533.
[56] M.J. Hostetler, A.C. Templeton, R.W. Murray, Langmuir 15 (1999) 3782.
[57] Y.J. Kim, Y.S. Yang, S.C. Ha, S.M. Cho, Y.S. Kim, H.Y. Kim, H. Yang, Y.T. Kim, Sens. Actuators B 106 (2005) 189.
[58] J. Lu, B. Kumar, M. Castro, J.-F. Feller, Sens. Actuators B 140 (2009) 451.